Published on Marine and Petroleum Geology

Available online 30 September 2016

http://dx.doi.org/10.1016/j.marpetgeo.2016.09.033

Does compaction-induced subsidence control accommodation space at the top of prograding carbonate platforms? Constraints from the numerical modelling of the Triassic Esino Limestone (Southern Alps, Italy)

Fabrizio Berra[a], Eugenio Carminati[b], Flavio Jadoul[a], Marco Binda[a]

[a] Università degli Studi di Milano, Dipartimento di Scienze della Terra "A. Desio", Milano, Italy

[b] Università di Roma "La Sapienza", Dipartimento di Scienze della Terra, Roma, Italy

Highlights

- *Various regressive facies are described on a high-relief carbonate platform.*
- *Facies distribution of regressive facies documents accommodation changes.*
- *Accommodation increases toward the prograding edge of the carbonate platform.*
- *Numerical modelling tests compaction of basinal sediments to create accommodation.*
- *Compaction of basinal sediments may control accommodation changes on the platform top.*

Keywords

Carbonate platform, Triassic, paleokarst, terra rossa soil, accommodation, differential compaction, numerical modelling

Abstract

The demise of the high-relief, steep-slope, prograding Ladinian-Early Carnian carbonate platforms of the Esino Limestone (Central Southern Alps of Italy) is marked by subaerial exposure of the platform top associated with different erosional (mainly karst-related), depositional and diagenetic processes (Calcare Rosso). The exposure-related deposits consist of three major facies associations: 1) residual soils with thin lenses of conglomerates with black pebbles, and, locally, weathered vulcanites; 2) chaotic breccia lenses irregularly distributed in the uppermost part of the Esino Limestone carbonate platform, interpreted as collapse breccias in karstic setting: 3) inter-supratidal carbonate cycles with dissolution and development of paleosols and tepee structures.

Facies distribution follows the sub-environments of the underlying Esino Limestone. Facies 1 and 2 typically characterize the core of the platform, covering the underlying inner platform facies. Facies 3 instead develops toward the edge of the platform, above reef-upper slope facies of the prograding facies of the Esino Limestone. The thickness of facies 3 decreases toward the core of the platform. Facies distribution reflects differences in the accommodation space and sedimentary processes from the rim (highest accommodation, favouring the deposition of peritidal-supratidal carbonates) to the core (reduced accommodation, causing pedogenesis and karstification) of the carbonate system.

The observed thickness changes may be controlled by different factors: 1) syndepositional tectonics, 2) subsidence induced by magmatic activity or 3) differential subsidence controlled by the stratigraphic architecture of the Esino Limestone platform and adjoining basins. As evidence of tectonics was not observed and the presence of volcanic bodies is only documented tens of km away from the study area, the scenario involving the creation of accommodation space by compaction of the basinal sediments (resedimented, fine-grained calciturbidites) during the progradation of the carbonate platform is here investigated. Numerical modelling was performed to verify the compatibility of compaction-induced subsidence with the observed depositional architecture. The models were built to simulate the architectural evolution of the platform by progressively adding layers from deepest to shallowest, while compacting the underlying sediments, in order to evaluate compaction-induced subsidence (and accommodation space for the Calcare Rosso) after the deposition of the youngest platform strata. Modelling results allow us to conclude that the wedge geometry of the Calcare Rosso, deposited on top of the extinct Esino carbonate platform, can be explained by subsidence controlled by compaction of the basinal sediments present below the early-cemented, fast prograding platform slope deposits.

1. Introduction

Subaerial exposure of the top of carbonate platform are typically marked by hiatuses associated with karst features (Esteban & Klappa, 1983). The entity, thickness of the platform affected by karst phenomena and facies (depositional vs. erosional/dissolution events) is controlled by different factors, such as duration of the subaerial exposure, amplitude of the relative sea-level fall, architecture of the exposed platform and climate conditions (typically controlling temperature and precipitations).

For bathymetric reasons, flat-topped, high-relief carbonate platforms are especially prone to record subaerial exposure events on wide areas. Karst features on high relief carbonate platforms, frequently marking the demise of carbonate platforms, have been observed and described both at surface and in subsurface.

To understand the processes that control the effects of the subaerial exposure and the distribution of the associated facies, which are extremely important for the hydrocarbon research as enhanced porosity is frequently associated with these surfaces, it is necessary to describe the types of karstic associations on a platform top and their areal distribution. The distribution of karstic associations is fundamental to identify local vs. regional factors controlling karst development. Changes in facies and thickness of karst deposits on the platform top may reflect uneven distribution of accommodation space of a carbonate system, able to enhance or smooth the effects of a sea-level fall. Distribution of accommodation space in a carbonate platform may be essentially controlled by syndepositional tectonics, magmatic activity and compaction-induced subsidence.

Compaction-induced subsidence, although less detectable from outcrop evidence, is most effective in high-relief prograding platforms, where early-lithified sediments prograde over unconsolidated basinal deposits (Hunt et al., 1996). Due to different compositions and early-diagenetic processes, carbonate platform and basinal sediments follow markedly different depth-porosity curves, basinal lithologies being more prone to compaction (Sclater and Christie, 1980; Goldhammer, 1997). The role of differential compaction in creation of accommodation space is known as an important factor potentially controlling the geometry of sedimentary wedges (e.g., Shinn & Robbin, 1983; Suppe, 1985; Doglioni & Goldhammer, 1988; Skuce, 1994; Carminati and Santantonio, 2010), and can be understood coupling numerical modelling with field observations. Differential compaction between reefal rocks and internal lagoon or slope sediments has been recognised either in the subsurface (e.g., the Devonian carbonate platform from Canada; Anderson & Franseen, 1991) or in outcrop (e.g., the Cretaceous-Oligocene Maiella Platform margin; Rusciadelli & Di Simone, 2007).

The distribution of different type of karst-related features on a prograding carbonate platform can mirror changes in accommodation space potentially resulting from differential compaction of basinal sediments. The demise of the high-relief, steep slope, prograding Ladinian-Early Carnian carbonate platforms of the Esino Limestone (Central Southern Alps of Italy) was triggered by a regressive event (Mutti, 1994; Gaetani et al., 1998; Berra, 2007), marked on the platform top by a subaerial exposure associated with different erosional (mainly karst-related), depositional and diagenetic processes (Calcare Rosso). Favourable exposures and a well-preserved platform architecture (Fig. 1) permit the reconstruction of the relationships between the carbonate platform facies deposited before the subaerial exposure and those related to the exposure event. This provides the opportunity, rare in the geological record, to unravel the possible relationships between the paleogeography of a high-relief carbonate platform and the types of karst features related to a sea-level fall. In this study, we discuss the importance of post-depositional compaction-related subsidence in the creation of accommodation space during the demise stage of the Ladinian Esino Limestone carbonate platform and evaluate its feasibility with ad-hoc numerical models.

2. Geological setting

The Southern Alps represent the south-verging part of the collisional Alpine belt (Handy et al, 2010), storing a Permian-Tertiary succession deposited after the Variscan orogeny (Bertotti et al., 1993; Berra & Carminati, 2010). The Late Anisian to Early Carnian succession of the Southern Alps is characterised by the presence of thick carbonate platform sediments separated by basinal troughs and seaways onto which they prograde (Fig. 1). These platforms, isolated toward the Dolomites, frequently merge into wider flat-topped carbonate platforms in Lombardy (Esino Limestone, Western Southern Alps; Fig. 1). The depositional architecture of the Lombardy platforms (Assereto & Casati, 1965; Assereto & Kendall, 1971; Assereto et al. 1977; Jadoul et al., 1992; Berra, 2007) reflects different evolutionary stages (Berra et al., 2011): an inception stage followed by an aggradational stage with increasing water depth in the basins and a later progradational stage. The flat-topped Esino Limestone platform reaches a maximum thickness of about 800 m and rapidly pinches out basinward with steep slopes (dipping about 35°) consisting of clinostratified breccias, with a platform to basin relief that reaches about 600-700 m (Berra et al., 2011).

This evolution reflects changes in accommodation space, which control the type and storage sites of the sediments produced by the carbonate factory as well as the geometry of the carbonate platform.

The aggradational stage of the Esino Limestone corresponds to reduced sedimentation in the basins (i.e. sediments are stored on the platform top) whereas during progradation resedimented limestones are more common in the basin (Berra et al., 2011).

Close to the Ladinian-Carnian boundary, a major sea-level fall is recorded in Lombardy by a lithostratigraphic unit characterised by regressive carbonate facies with evidence of subaerial exposures ("Calcare Rosso", Assereto et al., 1977; Assereto & Kendall, 1971; 1977; Assereto & Folk, 1980; Jadoul & Rossi 1982, Gaetani et al, 1998; Mutti, 1994; Berra, 2007; Vola & Jadoul, 2014), covering the flat top of the carbonate platform of the Esino Limestone. The Calcare Rosso builds a wedge, thickest (and well exposed) in middle Brembana Valley, where it consists of up to 60 m of cyclic peritidal limestones characterized by prevailing supratidal facies and evidence of multiple-stage karstification associated with lenses of carbonate breccias, precipitation of different generations of early carbonate-cement, internal sediments and development of mature tepees, loferitic breccias and terra rossa paleosols. The Calcare Rosso rapidly thins out northward to a few meters of red to grey paleosols and carbonate breccias, both related to superficial deposition and collapses of karst cavities. Locally (toward the east), volcanic deposits are present at the top of the Esino Limestone. The subaerial exposure of the Ladinian platforms can be traced, despite strong differences in thickness and facies associations, throughout the Lombardy Basin and probably all over the Southern Alps (Jadoul et al., 2002). Subaerial exposure rapidly halted the carbonate production on the platform top, while a major input of clay (probably reflecting a climate change and/or lowering of the base level) is recorded in the basin. Clay deposits onlap the slope of the previous carbonate system. The age of this event, constrained by biostratigraphic data in basinal successions (Balini et al., 2000), is early Carnian. Mutti (1994) interprets the Calcare Rosso as a complete third order sequence, bounded at the base and at the top by two major erosional surfaces that represent the sequence boundaries.

This fall in sea level occurring close to the Ladinian-Carnian boundary is well known in shallow-water carbonate platform settings of the western Southern Alps and produced a starvation episode in the basin (Berra, 2007; 2012) due to the demise of the carbonate platform caused by the subaerial exposure of the platform top. The amplitude of the sea-level fall is still debated: Assereto et al (1977) report the existence of karstic cavities up to 30-60 m from the platform top, Mutti (1994) suggests a sea-level drop of about 80 m, whereas new data (Binda, 2010) suggest a drop of around 20 m. The latter figure is compatible with a eustatic sea-level fall (limited to few tens of meters in a greenhouse interval as the Triassic), whereas the interpretation of Mutti (1994) requires a tectonic contribution (a 80 m eustatic sea-level drop is larger than any documented sea-level fall in the Triassic). Detailed sedimentological studies show that the different facies of the Calcare Rosso on

the platform top of the Esino Limestone are compatible with a sea-level fall not exceeding 20 m (Jadoul et al., 1992; Berra, 2007; Berra et al., 2011).

Due to the progradation of the Esino Limestone before the sea-level fall, the evidence of the subaerial exposure of the platform top is recorded on different facies of the Esino Limestone. Toward the core of the platform, exposure-related facies directly rest upon inner platform facies of the Esino Limestone, whereas toward the platform rims, the Calcare Rosso directly covers marginal or reefal facies. The exposure of different sub-environments of the Esino Limestone carbonate platform and the different facies related to the platform exposure open the possibility to verify the potential relationships between the depositional architecture of the Esino Limestone and the facies distribution in the Calcare Rosso and to identify the possible controlling factors.

3. Calcare Rosso: facies type, distribution and controlling processes

The Calcare Rosso unit, introduced by Assereto et al. (1977), classically defines an up to 60 m thick succession of cyclic peritidal limestone, rich in tepee structures, repeatedly capped by terra rossa paleosols, and filled by a great variety of fibrous-radial marine cements, and internal sediments. Recent geological mapping (ISPRA, 2012a) extended the definition of Calcare Rosso to different types of facies (mostly documented by residual breccias, karst features and dm-thick red clay deposits) that represent lateral, thinner equivalents of the classical Calcare Rosso.

The top of the Esino Limestone platform records spectacular evidence of ancient polyphase karst related to subaerial exposure of the carbonate platform, (Assereto & Kendall, 1977; Assereto, et al., 1977; Mutti, 1994; Vola & Jadoul, 2014). These papers focus on carbonate deposits affected by multiple karst and diagenetic episodes (typical facies of the Calcare Rosso). Field work and detailed stratigraphic and sedimentological observations led to the identification of three different exposure-related facies of the Calcare Rosso, preserved on the top of the Esino Limestone, whose paleogeographic distribution has been reconstructed. These exposure-related facies associations are:

- Type 1: residual soils (terra rossa type) and associated carbonate breccias;
- Type 2: chaotic breccia lenses irregularly distributed in the uppermost part of the Esino Limestone carbonate platform;
- Type 3: inter-supratidal carbonate cycles with dissolution structures and development of paleosols and tepee structures (typical facies of the Calcare Rosso).

3.1 Type 1) Residual breccia and red clay

This facies association is characterized by the occurrence, with different proportions, of intraformational breccias and red claystones (Fig. 2). The term residual breccias was introduced by Norton (1917) to describe breccia deposits developed on karst topographies.

The residual breccias generally consist of lenses of variable (0.3 to 4 m) thickness, with lateral extension up to tens of meters. Breccia lenses are massive, often amalgamated or poorly bedded (only the thicker deposits), locally with crude inverse or normal grading, associated with terra rossa horizons. Basal erosive contacts with underlying deposits and sharp and flat top boundary (Fig. 2) are common. Breccia deposits are often capped by faintly laminated calcarenites or millimetre-scale breccias (Fig. 2). Locally, yellow-greenish tuffaceous levels (<10 cm thick) and grey-dark grey wackestone and packstone (10-15 cm thick) are intercalated.

Pebbles (with a size ranging from 0.5 to 5 cm on average) consist of gray to dark gray limestones, from angular to sub-angular. Black micritic pebbles are locally present. The occurrence of asymmetric calcite crust in the lower part of the pebbles and the presence of blocky calcite indicate episodes of vadose circulation. The presence of crude bedding (marked by changes in the average size of the pebbles) in the conglomerate indicates a limited transport of the pebbles (subaerial sheet flows according to Assereto et al., 1977), which are generally poorly sorted. Locally, these breccias have a red clayey matrix (terra rossa). The conglomerate lenses are discontinuous and they can be laterally substituted by few decimeters-thick red clay with sparse carbonate pebbles. Conglomerates and red clay typically rest upon inner platform facies of the Esino limestone and are directly covered by peritidal facies (typically fenestral intraclastic pisoidal grainstone and stromatolitic bindstone affected by early dolomitization) recording the Early Carnian reprise of carbonate sedimentation (Breno Formation; Fig. 1).

The microfacies of the clasts consist of grey fenestral peloidal wackstone/packstone, boundstone, algal, oncoidal packstone/grainstone and dark-dark grey laminated limestone. The presence of subtidal and intertidal facies in the clasts suggests they may derive partly from the inner platform facies of the Esino Limestone and partly from the karstification and reworking of the Calcare Rosso.

The terra rossa layers and the red matrix consist of red clay containing abundant evidence of pedogenesis such as peds, clay matrix, iron-rich nodules and aggregates, illuvial clay, contractional fractures; Fig. 3). Locally, dolomitization is associated with the residual breccias (Fig. 2). The matrix of the residual breccias locally consists of reddish dolomitized microspar and green clay.

This facies association is characterized by rapid and sharp facies changes, but it can be followed in large parts of the flat-topped carbonate platform of the Esino Limestone. Locally, residual breccias

have been observed at the base of the typical facies of the Calcare Rosso, close to the prograding rims of the Esino Limestone platform.

3.2 Type 2) Endokarst on inner platform facies

The type 2 facies association, locally missing or strongly reduced, is frequently associated with cavities and fractures in the underlying uppermost part of the Esino Limestone, interpreted as endokarst features (Fig. 4). The most typical evidence for endokarst is represented by poorly-sorted, irregular breccia lenses consisting mostly of clasts of peritidal to shallow-subtidal facies of the Esino Limestone. These breccia lenses are directly cut in the upper part of the inner platform facies of the Esino Limestone and in a few (2-4) meters of peritidal-supratidal carbonates that are interpreted as the result of local deposition during the period of dominant subaerial exposure of the platform top. These irregular lenses, with an irregular geometry have been recognized up to about 20 m below the top of the Esino Limestone platform (Fig. 5). These breccias show sharp lateral transition to undisturbed peritidal facies of the Esino Limestone. The deepest part of these endokarst features consists of massive, clast-supported chaotic breccias. Collapsed and tilted m-scale strata surrounded by chaotic breccias can be recognized (Fig. 5). Toward the top, the breccias are characterized by the occurrence of a reddish clayey matrix and a general decrease in the size of the grains. The complex organization of these deposits as well as the presence of the peritidal-supratidal deposits at the top of the Esino Limestone suggest that several episodes of exposure and drowning affected the top of the high-relief platform of the Esino Limestone during development of the described karst-related features. The geometric distribution of the breccia bodies, their stratigraphic distribution and shape (V-shaped geometries) and the sedimentological features support their interpretation as a collapsed-paleocave system (Louks, 2007).

Locally, 10-15 cm large open fractures cut the underlying deposits for lengths up to 7-8 m. These fractures are frequently draped by centimetric crusts of isopachous cements and filled grey grainstone with rare bioclasts and fine reddish limestone. Re-opening of cavities and polyphasic filling by breccias originated from the walls of the cavities is interpreted as evidence of repeated exposure.

3.3 Type 3) Peritidal-supratidal carbonates affected by multiple subaerial exposures

This typical facies of the Calcare Rosso, up to about 60 m thick, has been the subject of detailed studies (Assereto, et al., 1977; Assereto & Kendall, 1977; Mutti, 1994; Vola & Jadoul, 2014). It bears the spectacular evidence of alternating carbonate deposition and subaerial exposures (Fig. 6), which generated rocks quarried since the Renaissance as decorative stone (known as Arabescato Orobico).

The unit is characterized by the presence of several unconformities marked by paleokarst and paleosols with terra rossa. These surfaces can be hierarchically arranged, identifying episodes of deposition, dissolution/karstification, calcite cement precipitation (Vola & Jadoul, 2014). The primary lithofacies of the Calcare Rosso are mainly composed of bedded peritidal limestones light grey, rarely dark grey, and pinkish-grey in color, with polychrome (red, yellow, pinky and dark grey) both concordant and discordant fractures and pockets. (Fig. 6). Subtidal/lagoonal facies are fossiliferous, with large cerithid gastropods, pelecypods, benthic foraminifera and small Dasycladacean algae (*Teutoporella echinata*, *Clypeina besici*). Rare undeterminable ammonoids have been found. Subtidal carbonates are deeply modified by karstification, pedogenesis and early diagenesis, showing horizons with tepee structures, loferitic breccias, sedimentary dikes with several generations of cements. Locally residual breccias (type 1 facies association) are present, typically at the base or where the unit thins out.

Upper and lower limits generally correspond to unconformities; the latter, in particular, is characterized by an evident regional disconformity with subaerial exposure, local karstification, and residual-collapse breccia lenses up to 10 m thick (Assereto et alii, 1977; Binda, 2010) (Fig. 2). Sedimentary dikes often penetrate for several meters downwards in the underlying platform, filling paleokarst pockets and fractures with terra-rossa sediments (Assereto et al., 1977; Binda, 2010; Berra et al., 2011; Vola & Jadoul, 2014). Some major, laterally continuous red paleosols represent marker horizons in the lower and middle part of the Calcare Rosso (Vola & Jadoul, 2014). The upper boundary with the Breno Fm is characterized by few decimeter-thick greenish to reddish marly clay intercalations associated with grey peritidal limestones that laterally pass to terra-rossa paleosols and grey supratidal limestones with tepees.

4. Relationships between facies and thickness

The distribution of the three different facies associations recognized in the Calcare Rosso identifies a regular distribution, allowing the identification of two main facies domains on the platform top: one characterized by the exclusive presence of facies associations 1 and 2 (residual soils and endokarst) and one dominated by the typical facies of the Calcare Rosso. These two domains are also characterized by a different thickness of the exposure-related deposits, ranging from 1 to 5 m on average for facies association 1 and 2 and up to 60 m for facies association 3 (Fig. 7). This difference permits, despite the irregular distribution of outcrops, the reconstruction of a map. The map highlights that the thickness change is gradual but not linear from the core of the platform top to the rims. The thickness remains roughly constant for most of the inner platform, whereas a relatively rapid increase is observed (from 3 m to 60 m) toward the edge of the underlying Esino Limestone platform, in a belt 1.5-6 km wide (Fig. 7). The relationships between facies association and thickness of the Calcare Rosso and of the subaerially-exposed flat top of the Esino Limestone document a strong link between the type of facies at the top of the Esino Limestone and the type of facies and thickness of the Calcare Rosso. The Calcare Rosso is thinner and represented by facies association 1 and 2 where resting above inner platform facies, whereas it increases in thickness and is represented by the typical facies 3 toward to the platform edge, where it covers open platform and reefal facies. These thickness and facies changes reflect changes in accommodation space in different sectors of the carbonate platforms, interacting with the sea-level fall responsible for the regional exposure of the platform top. Facies types record multiple subaerial exposures alternating with sedimentation where the Calcare Rosso is thickest, and a major subaerial exposure where it is thinnest. The observed alternation of sediment deposition and partial karstification in facies type 3 and absent or episodic deposition in facies type 1 and 2 can be explained suggesting the existence of high-frequency cycles with sea-level inundating the platform top where accommodation was higher (i.e. subsidence and sea-level fall curves frequently intersect) for facies type 3, but not able to flood the inner part of the platform where the rate of sea-level fall was higher than the subsidence (facies type 2 and 3; Fig.8)

As the depositional architecture of the Esino Limestone is characterized by a rapid progradation before the subaerial exposure of the platform top, the external part of the high-relief platform is characterized by a vertical evolution from basinal facies covered by slope breccia and, eventually, by reef facies, which are bordered, on the landward side, by high-energy, open platform facies. Inner platform facies at the core of the platform, instead, rest upon several hundred meters of peritidal carbonates, typically aggrading form the platform inception to the final subaerial exposure (Jadoul et al., 2002; Berra et al., 2011).

4.1 Facies distribution and controlling processes

The relationships between the exposure-related successions and the underlying platform suggests a strong control by the depositional architecture of the Esino Limestone on the facies distribution of the Calcare Rosso (Fig. 7). Accommodation space changed from the core of the Esino Limestone platform to its rims, where the Calcare Rosso reached its maximum thickness (60 m). The thickness change is associated with the change in facies association: the type 3 facies association dominates where the thickness of the units is higher than 5-10 meters, and most of the exposure-related succession is represented by peritidal-supratidal limestone affected by different degree of karstification. Residual facies (conglomerates and red clay, type 1 and 2 facies) dominate where the thickness is less than about 5 m. Three different processes could potentially control such gradual change in facies and thickness: 1) tectonics associated with the activity of faults inducing larger subsidence in a section of the carbonate platform or, alternatively, tilting of strata, 2) differential subsidence controlled by emplacement of magmatic bodies or 3) differential subsidence controlled by the different stratigraphic architecture of the internal vs. external (prograding) part of the platform.

Tectonic control can affect subsidence in two ways: a) generation of structural highs and lows by syndepositional faulting; or b) gentle tilting of large blocks along rotational faults. In case of syndepositional faulting, sharp changes in thickness are expected: this is in contrast with the field observations, as the change in thickness and facies is gradual. A differential subsidence controlled by a tilting may appear more compatible, but no evidence of tectonic tilting of the Esino Limestone (i.e. angular unconformity between Esino Limestone and overlying units) is observed.

Volcanic activity is documented in the sedimentary succession at the Ladinian-Carnian boundary by tuff layers and, locally, by primary volcanic products (ISPRA, 2012a). Significant early Carnian volcanic activity is documented ca 40 km east of the study area (ISPRA, 2012b), where intrusive and effusive rocks are preserved. However, in the study area up to 25 m of hyaloclastic deposits are preserved only in an area of about 1 km^2, close to the platform rim. The local distribution of these volcanic rocks and their reduced thickness and distribution suggest a limited, likely null, role in the control of differential subsidence. In addition, the distribution of the various facies of the Calcare Rosso seems to be independent from the position of the volcanic deposits, so that a role of the volcanic activity on the facies distribution can be excluded.

The evident relationship between the facies associations of the Calcare Rosso and the facies of the Esino Limestone suggests a role played by the architecture of the high-relief, flat-topped carbonate

platform. The architecture of the Esino Limestone is characterized at a regional scale by the rapid progradation of slope facies toward the basin (Jadoul et al., 1992; Berra, 2007; Berra et al., 2011). The prograding slope facies consist of clast-supported, early-cemented breccias (Jadoul & Frisia, 1988; Frisia-Bruni et al., 1989) prograding on basinal fine-grained turbidites (Jadoul et al., 1992; Berra et al., 2011). This architecture is responsible for the progradation of these breccia bodies above 100 m to more than 200 m thick fine-grained basinal calciturbidites (Fig. 9), observed where the base of the prograding platform is preserved (e.g. Berra, 2007; Berra et al., 2011). Unfortunately, below the prograding facies of the Esino Limestone covered by the thickest succession of the Calcare Rosso, basinal facies do not crop out. Here, it is therefore impossible to measure the thickness of the basinal succession. Nevertheless, local evidence (the presence of a thick succession of Carnian deposits filling an inherited depression just south of the study area; Garzanti & Jadoul, 1985; ISPRA, 2012a) as well as the regional evolution of the platform suggest the presence of a basinal succession from 100 to 200 m thick, similar to that observed in all the prograding flanks of the Esino Limestone. Considering this as a present thickness, we can expect that the uncompacted thickness of the basinal succession was higher and an original thickness from about 150 m to about 300 m was consequently assumed in the following numerical modelling. These basinal facies (mostly wackestone and packstone) underwent rapid and considerable compaction. This is documented by microfacies observations from the fine-grained, bedded basinal limestone (Fig. 9), indicating that compaction of the basinal sediments is strongly controlled by the nature of the sediments and by the microfacies type (Fig. 9). The differential compaction of these basinal sediments likely produced the changes in the accommodation space of the Calcare Rosso, as discussed in the following section.

5. Numerical models of creation of accommodation space induced by compaction

5.1 Modelling technique

Different models were built to simulate the evolution (aggradation and progradation) of the Esino carbonate platform by progressively adding layers from deepest to shallowest, while compacting the underlying sediments, in order to evaluate subsidence (and accommodation space for the Calcare Rosso) due to compaction after the deposition of the youngest strata and the demise of the carbonate platform (Fig. 10). Our model geometry (Fig. 11) was based on the 2D reconstruction of the

geometry of the platform-basin system shown in Fig. 1. Owing to early cementation, the Esino limestone is assumed as uncompactable, whereas, during deposition of the Esino Limestone, the basinal sediments are progressively compacted.

The compaction procedure is applied to 1D successions of sedimentary strata. The distance domain of the basin (x) is discretized every 10 m. Our models do not account for the effect of water load on compaction. We assume that compaction of the basinal sediments is exclusively depth-dependent. Compaction should have occurred progressively during the deposition of carbonate platform (assumption widely accepted and utilized in the literature, since it is consistent with studies on carbonates in the offshore of south Florida, where porosity reduction is mainly depth-controlled; Schmoker & Halley, 1982) or immediately after (the fluid overpressures observed in many basins worldwide are frequently associated with the occurrence of undercompacted sediments, testifying for the time-dependent nature of compaction). For example, Dugan & Flemings (2000) demonstrated that fluid overpressure in undercompacted Miocene-Pliocene sediment in the offshore of New Jersey are the result of rapid Pleistocene sedimentation load. Although the time-dependence of soft sediment mechanics is not addressed in our simulations, the results for the five units modelled show two end members (or scenarios). For unit 1 to 4 (deposited during a period of constant or rising sea-level) the two scenarios do not create different geometries, as all the accommodation space created on the platform top by compaction of basinal sediments is expected to be immediately filled by the carbonates produced on the platform top. The expected geometry is flat-topped, up to the sea-level, independently on the time of subsidence. For unit 5, modelled during the sea-level fall, the situation is different. The topmost black solid line (figs 12 to 15) represents the geometry of the platform top assuming that compaction of basinal sediments completely occurred during deposition (first scenario). In this case, no compaction related subsidence is predicted after the deposition as the accommodation space produced by the compaction of basinal sediments is immediately filled by the carbonate produced on the platform top. In a second scenario, the compaction associated with the deposition of the shallowest unit of the Esino Limestone is assumed to have occurred after the demise of the carbonate platform. In other words, the unit number 5 of the Esino Limestone is assumed to have deposited flat from the internal lagoon to the rim and progressively downtilted and deformed by the following compaction-related subsidence, with no sedimentation on the part of the platform top exposed as a consequence of the sea-level fall. The red line (figs 12 to 15) shows the geometry of the top of this unit after the compaction of the basinal sediments. A similar geometry will not be preserved if the sea-level remains constant or rises (units 1 to 4, as the created accommodation space is filled by sediments

produced on the platform top) whereas, if sea-level falls, the basinward-dipping geometry of the platform top is preserved on the exposed part of the platform (unit number 5).

As it will be discussed, this post-depositional subsidence is proposed to be the possible origin of the development of accommodation space for the Calcare Rosso.

To simulate compaction, we adopt Athy's (1930) exponential porosity vs. depth relationship:

$$\phi=\phi_0 \exp^{-cy}, \quad (1)$$

where ϕ is the porosity associated with a sedimentary load of y (in kilometers), ϕ_0 is the porosity of a specific lithology at its deposition, and c is coefficient generally derived from measurement of porosity at different depths in boreholes. In order to analyze the sensitivity of the models to the lithology of the basinal sediments, we performed simulations assuming the parameters, taken from Sclater & Christie (1980) of chalk (highly-compactable sediments; ϕ_0= 0.7 and c = 0.71), and sand (less-compactable sediments; ϕ_0= 0.49 and c = 0.27). These lithologies can be considered as upper and lower bounds for basinal sediments compaction. In addition to these parameters from the literature, which were adopted to evaluate the potential range of variation of generation of accommodation space, ad hoc compaction parameters were calculated. These were calculated using the method of Hölzel et al. (2008), by arithmetically averaging (weighted average) the parameters of each lithology occurring in the deep-sea sediments. The calculated parameters are listed in Table 1 and are consistent with those calculated by Berra and Carminati (2010) for the same succession. Owing to the variability of the basinal units (Fig. 9), in a first case these sediments were considered (micrites and pelites) slightly less compactable than chalk. These compaction parameters are intended to simulate the behavior of very fine sediments deposited in distal areas (i.e., far from the prograding slope, where the input from the prograding platform is reduced). Owing to the presence in the study area of a significant amount of calcarenites in the basinal facies proximal to the prograding slopes (coarser sediments, where the influx of the prograding platform is higher), in a second case compaction parameters were calculated assuming a combination of coarser and less compactable lithologies (mudstone, calcarenites and pelites).

Another uncertainty concerns the maximum thickness of the compactable basinal sediments, as discussed earlier. For this reason, we simulated the evolution for two scenarios, characterized by maximum original thicknesses of compactable sediments of 150 m and 300 m respectively.

Because of the relatively small lateral extent of the model (few km), no isostatic corrections were applied. This choice is supported by the observation that the lithosphere does not flex under laterally small loads (Turcotte & Schubert, 2002).

5.2 Modelling results

Figures 12 to 15 show the modelled geometry of the Esino carbonate platform and of the adjoining deep-sea basin for the scenarios characterized by 150 m and 300 m thick basinal sediments. Figures 12 and 14 show the results assuming, in the compactable basin, sand and chalk lithologies taken from the literature, whereas figures 13 and 15 were produced assuming ad-hoc parameters for the Central Southern Alps, simulating proximal and distal basinal facies (Table 1). In the first case, no compaction related subsidence is predicted after the deposition of unit 5, whereas for the second scenario, post-deposition compaction related subsidence is portrayed in panel a and c of both figures.

Considering the scenario with 150 m thick compactable sediments (Figs. 12 and 13), all four cases predict ca. 10 meters of compaction-related subsidence in the portion of the model above the inner platform of unit 4 and a subsidence sag from the platform-break of the top of unit 4 outward. Maximum subsidence is predicted in correspondence with the platform-break of the top of unit 5 (maximum thickness, i.e. load, of the carbonate platform facies). The inner platform portion of the model affected by subsidence (progressively decreasing toward the center of the platform) is ca. 1 km wide. Minimum subsidence peak values of 30 m are predicted for sandy basinal sediments, whereas adopting chalk parameters, peak subsidence is ca 100 m. Peak values of 75 m and 90 m are predicted using ad-hoc parameters simulating proximal and distal basinal sediments respectively.

Considering the scenario with 300 m thick compactable sediments (Figs. 14 and 15), similar subsidence patterns are observed, but the magnitudes of peak subsidence are larger. Minimum subsidence peak values of 40 m are predicted for sandy basinal sediments, whereas adopting chalk parameters, peak subsidence is ca 140 m. Peak values of 110 m and 130 m are predicted using ad-hoc parameters simulating proximal and distal basinal sediments respectively.

6. Discussion

Similarly to what suggested by Doglioni and Goldhammer (1988) for Carnian deposits in the Eastern Southern Alps (Dolomite region), we propose that the observed accommodation space for the deposition of the wedge-shaped Calcare Rosso could be totally provided by compaction-related subsidence induced by the progradation of the early-cemented, uncompactable Esino carbonate platform onto compactable deep-sea sediments. The role of compaction on the growth-mode of the Esino Limestone has been recently investigated by Berra & Carminati (2012) who showed that the

presence of early fractures oriented parallel to the platform in the upper slope facies rim could be related to the differential compaction of the basinal facies underlying the prograding slope.

The geometry and thickness of the Calcare Rosso are consistent with our modelling results. This formation is thickest at the lateral edge of the Esino carbonate platform and thins out towards the platform interior, similarly to model-predicted compaction-related subsidence, which is maximum at the platform-break at the top of unit 5 and decreases towards the platform internal part. Indeed the Calcare Rosso thins from about 60 m to less than 10 m in 1.5 to 6 km, whereas in our model the decrease of subsidence occurs in ca. 1 km. If part of compaction was not accommodated during the deposition of units 1-4, the area characterised by post-depositional subsidence would be larger. The maximum amount of subsidence predicted by models (between 75 and m and 90 m and between 110 m and 130 m considering ad-hoc realistic compaction parameters for the 150 m and 300 m basinal sediments thick scenarios, respectively) is consistent with the distribution of Calcare Rosso in the field. Although these subsidence figures are larger than the maximum thickness (around 60 m) of the Calcare Rosso, it has to be considered that our model assumes that the creation of accommodation space occurred immediately after the deposition of unit 5. In reality, it is possible that only a part of the total compaction occurred after the deposition of unit 5, so that only a percentage of it (30-40% in case of the thicker basinal succession; 15-20% in case of thinner basinal succession) contributed to the creation of the accommodation space for the Calcare Rosso. This observation suggests that, according to the thickness of the basinal successions used in the model, the process of compaction probably lasted along a larger time span, continuing after the end of the deposition of the Calcare Rosso. The existence of compaction-induced subsidence lasting longer than the time of deposition of the Calcare Rosso is supported by the carbonate succession (Breno Formation) that records the return to peritidal deposition after the sea-level fall recorded by the Calcare Rosso. The Breno Formation, directly covering the different facies of the Calcare Rosso, is thicker above the prograding facies of the Esino Limestone, whereas it is thinner where deposited on the inner platform facies of the Esino Limestone, where the Calcare Rosso is represented by facies type 1 and 2.

7. Conclusions

When gradual changes in the thickness and facies distribution of karst-related facies on a flat-topped, high-relief carbonate platform are in tune with changes in the facies of the underlying platform, it is possible to verify any possible control by the depositional architecture of the exposed platform. In the Southern Alps of Italy, the subaerially-exposed Esino Limestone shows higher

accommodation space on the prograding edge of the platform (covering basinal fine-grained calciturbidites) with respect to its core: this change is recorded by the Calcare Rosso, increasing in thickness from 0 to 5 meters in the core of the platform to about 60 m toward the rim. To verify the possible contribution of compaction-induced subsidence above the prograding slope facies of the Esino Limestone, numerical models were developed, considering different scenarios. The results strongly support the hypothesis that compaction induced subsidence could explain both the changes in thickness of the Esino Limestone and its relationships with the stratigraphic evolution of the underlying platform. Field data and modelling suggest that the process of sediment compaction under a prograding platform could be a relatively gradual process, able to explain thickness changes also in younger successions. Compaction thus results to be an important process to explain changes in the distribution of accommodation spaces in depositional settings of known architecture.

Acknowledgements

Funding from PRIN 2010-2011 (Project 20107ESMX9: ”Crisi e ripresa di sistemi carbonatici e potenziale per la formazione di reservoir: i ruoli di clima, tettonica e magmatismo) and Progetti di Ateneo 2014 by Sapienza University is acknowledged. We would like to thank Wolfgang Blendinger for the conceptual comments and Giuseppe Rusciadelli for his detailed and constructive critics: their contributions, together with those of the Associate Editor Piero Gianolla, improved the original version of this paper.

References

Anderson, N.L., Franseen, E.K., 1991. Differential compaction of Winnipegosis reefs: A seismic perspective. Geophysics, 56, 142–147.

Assereto, R., Casati, P., 1965. Revisione della stratigrafia permotriassica della Val Camonica meridionale (Lombardia). Riv. It. Paleont. Strat., 71, 999–1097.

Assereto, R., Folk, R.L., 1980. Diagenetic fabric of aragonite, calcite and dolomite in an ancient peritidal-spelean environment: Triassic Calcare Rosso, Lombardia, Italy. J. Sedim. Petrol., 50: 371-394, Tulsa.

Assereto, R., Kendall, C.G.ST.C., 1971. Megapolygons in Ladinian limestones of Triassic of Southern Alps: evidence of deformation by penecontemporaneous desiccation and cementation. 1. Sediment. Petrol. 43, 715-723 (1971).

Assereto, R., Kendall, C.G.ST.C., 1977. Nature, origin and classification of peritidal tepee structures and relative breccias. Sedimentology, 24: 153-210, Oxford.

Assereto, R., Jadoul, F., Omenetto, P., 1977. Stratigrafia e metallogenesi del settore occidentale del distretto a Pb, Zn, fluorite e barite di Gorno (Alpi Bergamasche). Riv. It. Paleont. Strat., 83, 395-532.

Athy, L.F., 1930. Density, porosity and compaction of sedimentary rocks: Am. Ass. Petr. Geol. Bull., 14, 1–24.

Balini, M., Germani, D., Nicora, A., Rizzi, E., 2000. Ladinian/Carnian ammonoids and conodonts from the classic Schilpario-Pizzo Camino area (Lombardy): revaluation of the biostratigraphic support to chronostratigraphy and paleogeography. Rivista Italiana di Paleontologia e Stratigrafia (Research In Paleontology and Stratigraphy), 106, 19-58.

Berra, F., 2007. Sedimentation in shallow to deep water carbonate environments across a sequence boundary: effects of a fall in sea level on the evolution of a carbonate system (Ladinian-Carnian, eastern Lombardy, Italy). Sedimentology, 54, 721-735.

Berra, F., Carminati, E., 2010. Subsidence history from backstripping analysis of the Permo-Mesozoic succession of the Central Southern Alps (Northern Italy), Basin Res., 22, 952–975.

Berra, F., Carminati, E., 2012. Differential compaction and early rock fracturing in high‐relief carbonate platforms: numerical modelling of a Triassic case study (Esino Limestone, Central Southern Alps, Italy). Basin Research, 24(5), 598-614.

Berra, F., Jadoul, F., Binda, M., Lanfranchi, A., 2011. Large-scale progradation, demise and rebirth of a high relief, flat-topped carbonate factory (Late Anisian-Early Carnian, Lombardy Southern Alps, Italy). Sed. Geol., doi: 10.1016/j.sedgeo.2011.05.002.

Berra, F., 2012. Sea-level fall, carbonate production, rainy days: how do they relate? Insight from Triassic carbonate platforms (Western Tethys, Southern Alps, Italy). Geology, 40(3), 271-274.

Bertotti, G., Picotti, V., Bernoulli, D., Castellarin, A., 1993. From Rifting to Drifting: Tectonic Evolution of the South Alpine Upper Crust from Triassic to Early Cretaceous. Sed. Geol., 86, 53-76.

Binda, M, 2010. Facies distribution of a rimmed carbonate platform and overlying regressive carbonates: the Esino Limestone and Calcare Rosso facies in the Central Southern Alps (Lombardy, Italy). PhD Thesis, University of Milan.

Carminati, E., Santantonio, M., 2005. Control of differential compaction on the geometry of sediments onlapping paleoescarpments: insights from field geology (Central Apennines, Italy) and numerical modelling Geology, 33, 353-356.

Doglioni C., Goldhammer R.K., 1988. Compaction-induced Subsidence in a margin of a carbonate platform. Basin Res., 1/4, 237-246.

Dugan, B., Flemings, P.B., 2000. Overpressure and Fluid Flow in the New Jersey Continental Slope: Implications for Slope Failure and Cold Seeps, Science, 288, 289-291.

Esteban, M. Klappa, C. F., 1983. Subaerial Exposure Environment. In: Scholle, P. et al. (eds.): Carbonate Depositional Environments. Amer. Assoc. Petrol. Geol. Memoir 33, Tulsa, 254.

Frisia-Bruni, S., Jadoul, F., Weissert, H., 1989. Evinosponges in the Triassic Esino Limestone (Southern Alps): documentation of early lithification and late diagenetic overprint. Sedimentology 36, 685–699.

Garzanti E., Jadoul F. 1985. Stratigrafia e paleogeografia del Carnico lombardo (sondaggio S. Gallo, Val Brembana). Riv. It. Pal. Strat., 91 (3): 295-320,

Gaetani, M., Gnaccolini, M., Jadoul, F., Garzanti, E., 1998. Multiorder sequence stratigraphy in the Triassic system of the Western Southern Alps. In: Mesozoic and Cenozoic Sequence Stratigraphy of European Basins (Ed. by P.C. de Graciansky, J. Hardenbol, T. Jacquin and P.R. Vail), SEPM Spec. Publ., 60, 701–717.

Goldhammer, R.K., 1997. Compaction and decompaction algorithms for sedimentary carbonates, Journal of Sedimentary Research, 67, 26-35.

Handy, M.R., Schmid, S.M., Bousquet, R., Kissling, E., Bernoulli, D., 2010. Reconciling plate-tectonic reconstructions of Alpine Tethys with the geological–geophysical record of spreading and subduction in the Alps, Earth-Science Reviews, 102, 121-158, DOI:dx.doi.org/10.1016/j.earscirev.2010.06.002.

Hölzel, M., Faber, R., Wagreich, M., 2008. DeCompactionTool: Software for subsidence analysis including statistical error quantification. Comput. Geosci. 34, 1454-1460.

Hunt, D., Allsop, T., Swarbrick, R.E., 1996. Compaction as a primary control on the architecture and development of depositional sequences: conceptual framework, applications and implications, in: High Resolution Sequence Stratigraphy: Innovations and Applications (Ed by J. Howell and J.F. Aitken), Geol. Soc. Lond., 104, 321-345.

ISPRA 2012a. Foglio 077 Clusone, Carta Geologica d'Italia 1:50.000.

ISPRA 2012b. Foglio 099 Iseo, Carta Geologica d'Italia 1:50.000.

Jadoul, F., Frisia, S., 1988. Le evinosponge: ipotesi genetiche di cementi calcitici di cavità nella piattaforma ladinica delle Prealpi Lombarde (Alpi Meridionali). Riv. It. Paleont. Strat. 94, 81–104.

Jadoul F., Gervasutti M., Fantini Sestini N., 1992. The Middle Triassic of the Brembana Valley: preliminary study of the Esino Platform evolution (Bergamasc Alps). Riv. It. Paleont. Strat., 98, 299-324.

Jadoul, F., Rossi, P.M., 1982. Evoluzione paleogeografico- strutturale e vulcanismo triassico nella Lombardia centro-occidentale. In: Guida alla geologia del Sudalpino centro-occidentale (Ed. by A. Castellarin and G.B. Vai), Guide Geol. Reg. S.G.I, 143-155.

Jadoul, F., Nicora, A., Ortenzi, A., Pohar, C., 2002). Ladinian stratigraphy and paleogeography of the Southern Val Canale (Pontebbano-Tarvisiano, Julian Alps, Italy). Memorie della Societa Geologica Italiana, 57(1), 29-43.

Loucks, R.G., 2007. A review of coalesced, collapsed-paleocave systems and associated suprastratal deformation. Acta Carsologica 36, 121–132.

Mutti, M., 1994. Association of tepees and paleokarsts in the Ladinian Calcare Rosso (Southern Alps, Italy). Sedimentology, 41, 621-641.

Norton, W. H., 1917). A classification of breccias. The Journal of Geology, 25(2), 160-194.

Rusciadelli G., Di Simone S., 2007. Differential compaction as control on depositional architectures across the Maiella carbonate platform margin (central Apennines, Italy). Sed. Geol., 196, 133- 155.

Schmoker, J.W., Halley, R.B., 1982. Carbonate porosity versus depth: A predictable relation for south Florida. Am. Ass. Petr. Geol. Bulletin, 66, 2561–2570.

Sclater, J.G., Christie, P.A.F., 1980. Continental stretching: an explanation of the post–mid-Cretaceous subsidence of the central North Sea basin. J. of Geophys. Res., 85, 3711–3739.

Shinn, E.A., Robbin, D.M., 1983. Mechanical and chemical compaction in fine-grained shallow-water limestones. J. Sed. Petr., 53, 595-618.

Skuce, A.G., 1994. A structural model of a graben boundary fault system, Sirte Basin, Libya. Canadian J. of Exploration Geophys., 30, 73-83

Suppe, J., 1985. Principles of structural geology, pp. 537, Prentiede-hall, Princeton

Taylor, J.M., 1950. Pore-space reduction in sandstones. AAPG bulletin, 34, 701-716.

Turcotte, D.L., Schubert, G., 2002. Geodynamics (2nd edition). Cambridge University Press, Cambridge.

Vola, G., Jadoul, F., 2014. Applied stratigraphy and carbonate petrography of the Arabescato Orobico dimension stone from the Bergamasc Alps (Calcare Rosso, Italy). Italian Journal of Geosciences, 133(2), 294-314.

Figure captions

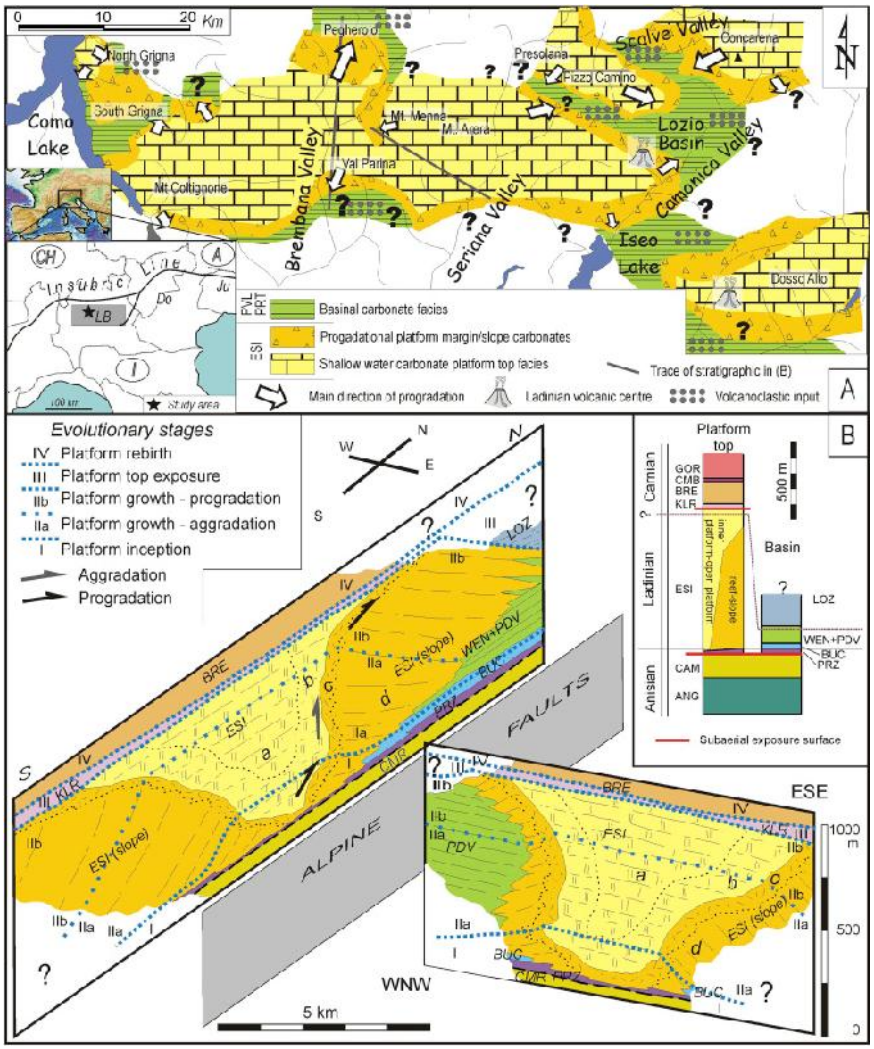

Fig. 1 – Geological setting of the studied succession (modified after Berra et al., 2011): A. Paleogeographic distribution of the carbonate highs and intraplatform basins in the Lombardy Basin at the end of the deposition of the Esino Limestone. In the inset: LB: Lombardy Basin; Do: Dolomites; Ju: Julian Alps. B) Schematic facies distribution along two stratigraphic sections across the study area (Pegherolo Massif–Middle Val Brembana). The trace of the stratigraphic sections is shown in (A). On the top right, a simplified stratigraphic diagram summarizes the stratigraphy in basinal (right) and platform top (left) settings. ANG: Angolo Limestone; CAM: Camorelli Limestone; PRZ: Prezzo Limestone; BUC: Buchenstein Fm.; PDV: Perledo-Varenna Limestone; WEN: Wengen Formation; ESI: Esino Limestone, consisting of: a) bedded inner platform facies; b) massive bioclastic facies (open platform); c) reef belt; d) slope breccias; KLR: Calcare Rosso; LOZ: Lozio Shale; BRE: Breno Formation; CMB: Calcare Metallifero Bergamasco; GOR: Gorno Formation.

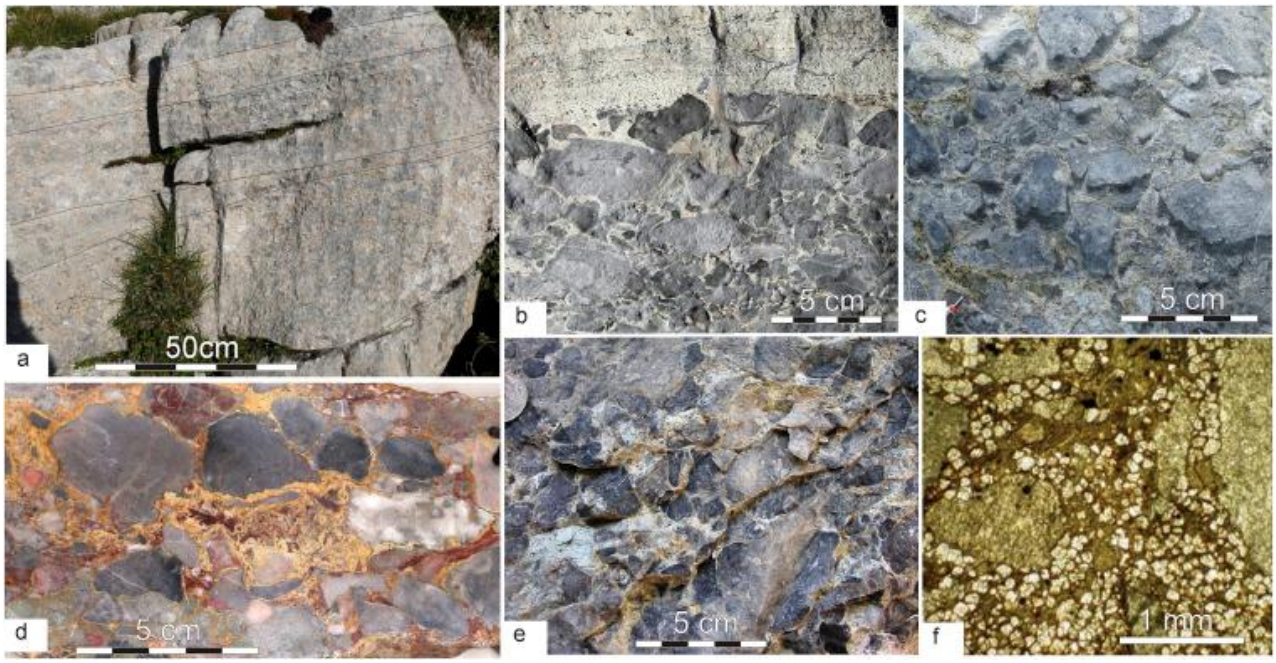

Fig. 2: Aspects of type 1 facies association: a- Lenticular, poorly bedded breccia bed with erosional base (Mt. Arera) and faint laminations; b- Clasts-supported breccia with black pebbles with a marly matrix sharply covered by a mud-supported fine-grained breccia with angular black pebbles (Mt. Arera); c- Carbonate breccias with clasts asymmetrically bordered by black pendant cements (Mt. Pegherolo); d- Clast-supported breccia with poorly-sorted clasts of different types of carbonates and Terra Rossa paleosols (Val Mora); e- Poorly-sorted, clast-supproted breccia dominated byblack pebbles, with a greenish clayey matrix (Monte Trevasco); f- Photomicrograph of a residual breccia: clasts show dissolution, dolomitization in the marly matrix.

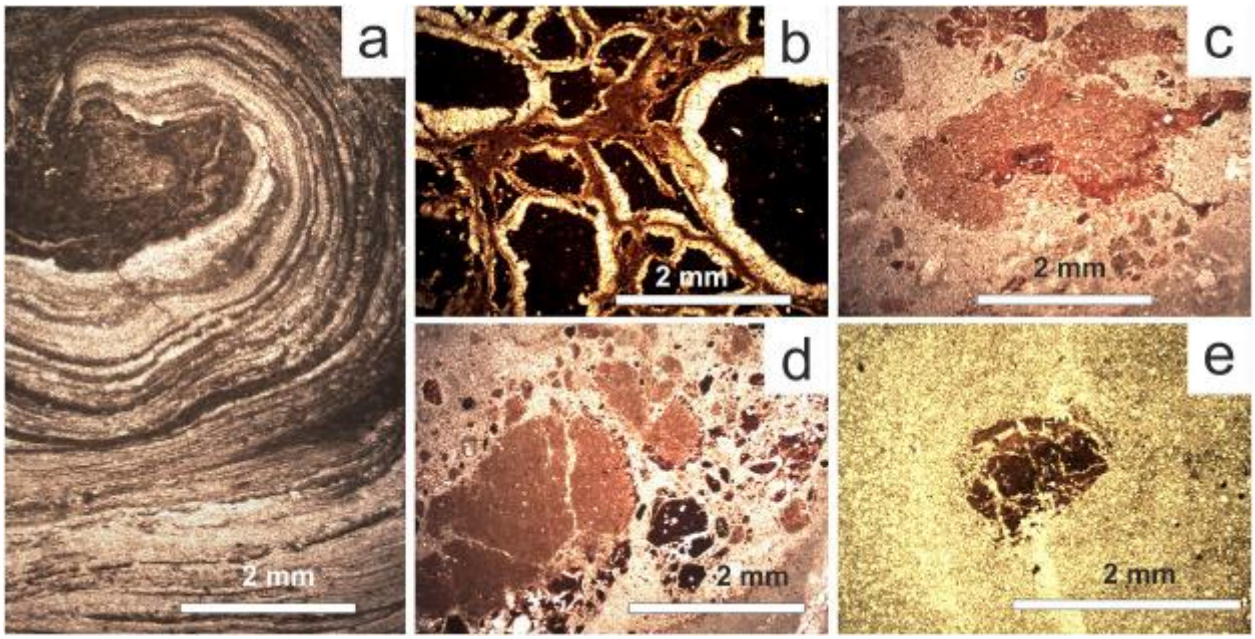

Fig. 3 - Microphotographs of thin section from the different facies type of the Calcare Rosso. a) pisoid in the supratidal limestone of type 3 facies association; b) iron rich subangular peds coated by calcite in a clay matrix; c) red clay aggregate in a residual breccia with carbonate clasts; d) fractured, rounded clay aggregate, with darker iron-rich rims (bottom) and grains; e) fractured subspherical accumulation of illuviated clay in a dolomitized carbonate.

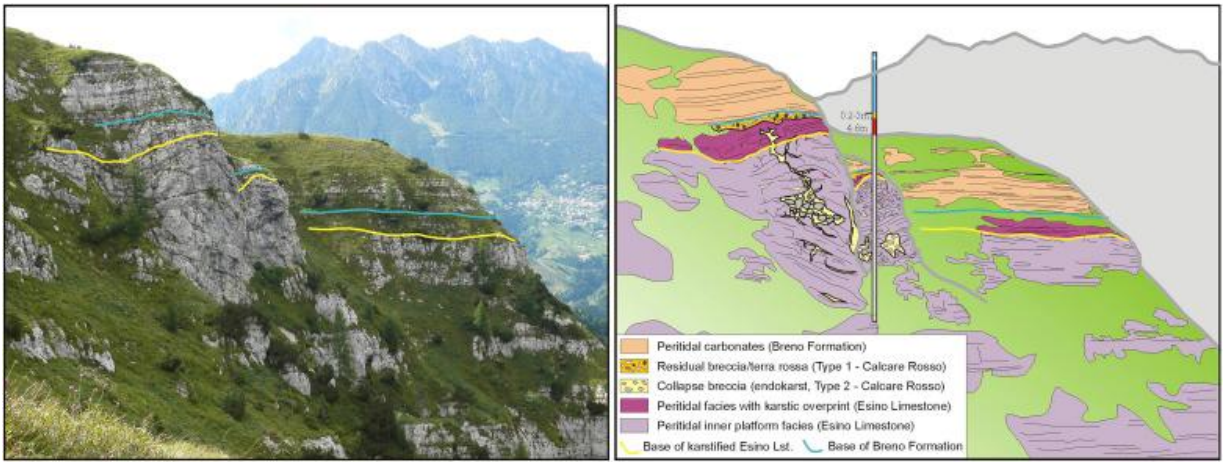

Fig. 4 - Endokarst (type 2 facies association) in the upper Esino Limestone: on the left panoramic view of the transition between Esino Limestone and Breno Formation, with the karst-related residual breccia layers of the Calcare Rosso. On the right, line drawing of the same image.

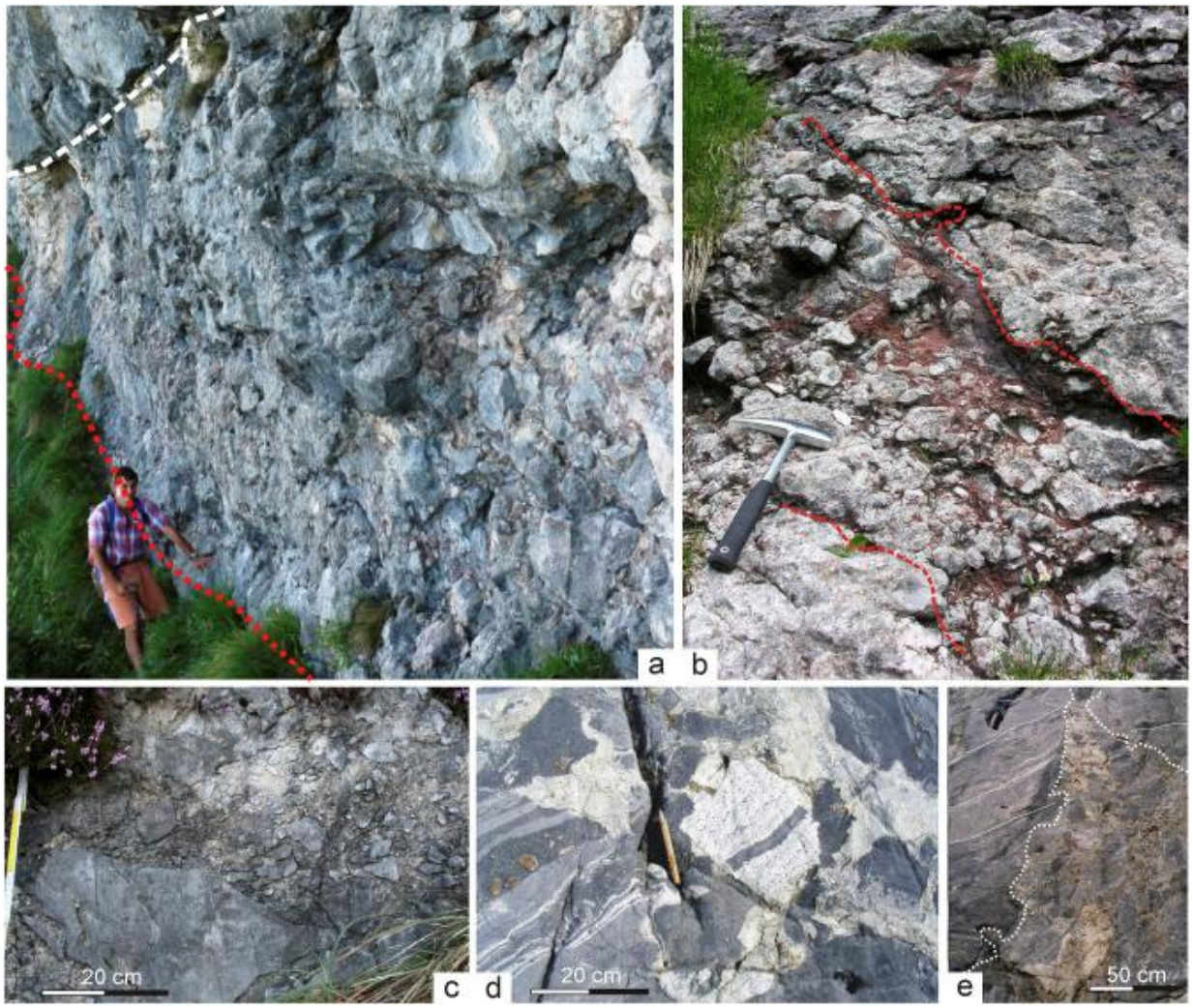

Fig. 5 – Aspects of type 1 facies and facies 2 associations: a) massive, clast-supported, lenticular breccia body at the top of the peritidal facies of the Calcare di Esino, consisting of clasts derived from the Calcare di Esino, with a terra rossa matrix; b) detail of a thin breccia layer with abundant terra rossa matrix at the top of the Calcare di Esino; c) monospecific breccia with unsorted angular clasts (collapse breccia); d) collapse breccia in peritidal facies with fenestral fabric; e) vertical shaft in bedded peritidal facies (uppermost Esino Limestone) filled by angular, local carbonate clasts.

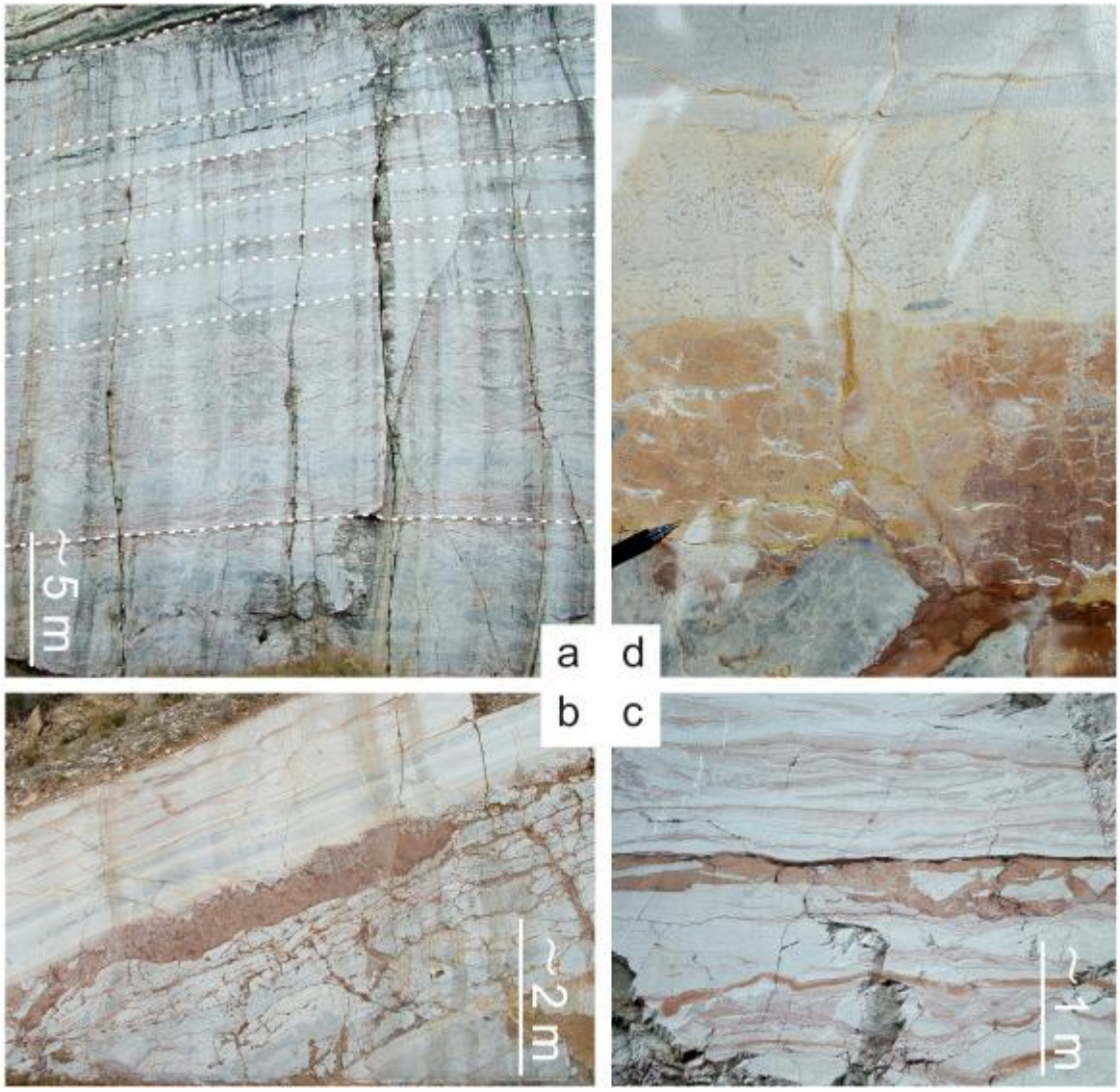

Fig. 6 – Type 3 facies association: a) vies of a quarry wall cut in the middle-upper part of the Calcare Rosso, note the presence of several subaerial exposure surfaces (marked by tepees and terra rossa deposits) bounding episodes of carbonate sedimentation; b) detail of one of the paleosol in the lower part of the Calcare Rosso: note the alteration of the first meters below the terra rossa layer, with fractures filled by terra rossa, above the terra rossa layer a transgression is recorded by deposition of peritidal carbonates; c) detail of the terra rossa layer with angular clasts; d) detail of the transition between a terra rossa pedogenic layer (below) ant fenestral peritidal carbonates marking a return to marine conditions (above).

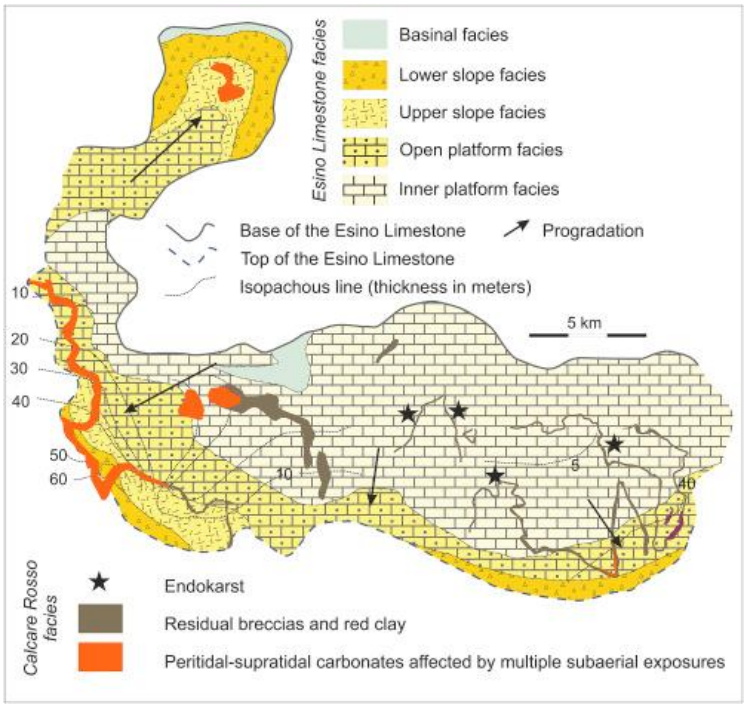

Fig. 7 – Tentative paleoeographic map of the facies distribution in the Esino Limestone and in the Calcare Rosso, showing the thickness of the karst-related facies and the distribution of the endokarst deposits.

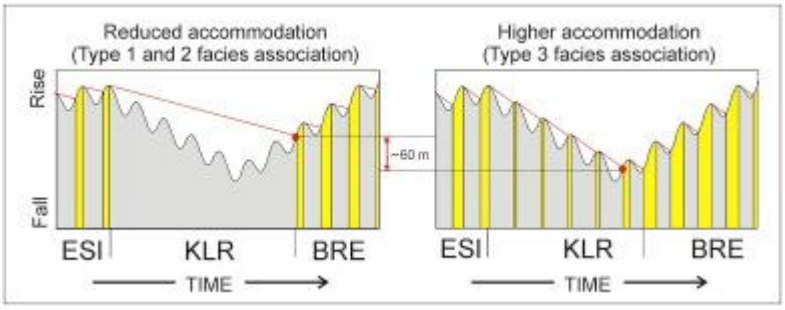

Fig. 8 – Conceptual model for describing the observed different facies types and thickness of the Calcare Rosso (the yellow fill represents periods of deposition, the light gray fills corresponds to intervals of non-deposition/erosion). Left: where accommodation is reduced (the red lines are less steep), facies 1 and 2 dominate as the platform top remains subaerially exposed for most of the time corresponding to the deposition of the Calcare Rosso. Right: where accommodation is higher (the red lines are steeper), facies 3 dominates and the higher accommodation space creates the conditions of multiple events of flooding and exposure of the platform top during higher-frequency sea-level cycles. A difference in accommodation (about 60) m is expected in the two different conditions. Note that this conceptual model implies that the beginning of the deposition of the Breno Formation is younger in the more subsiding area.

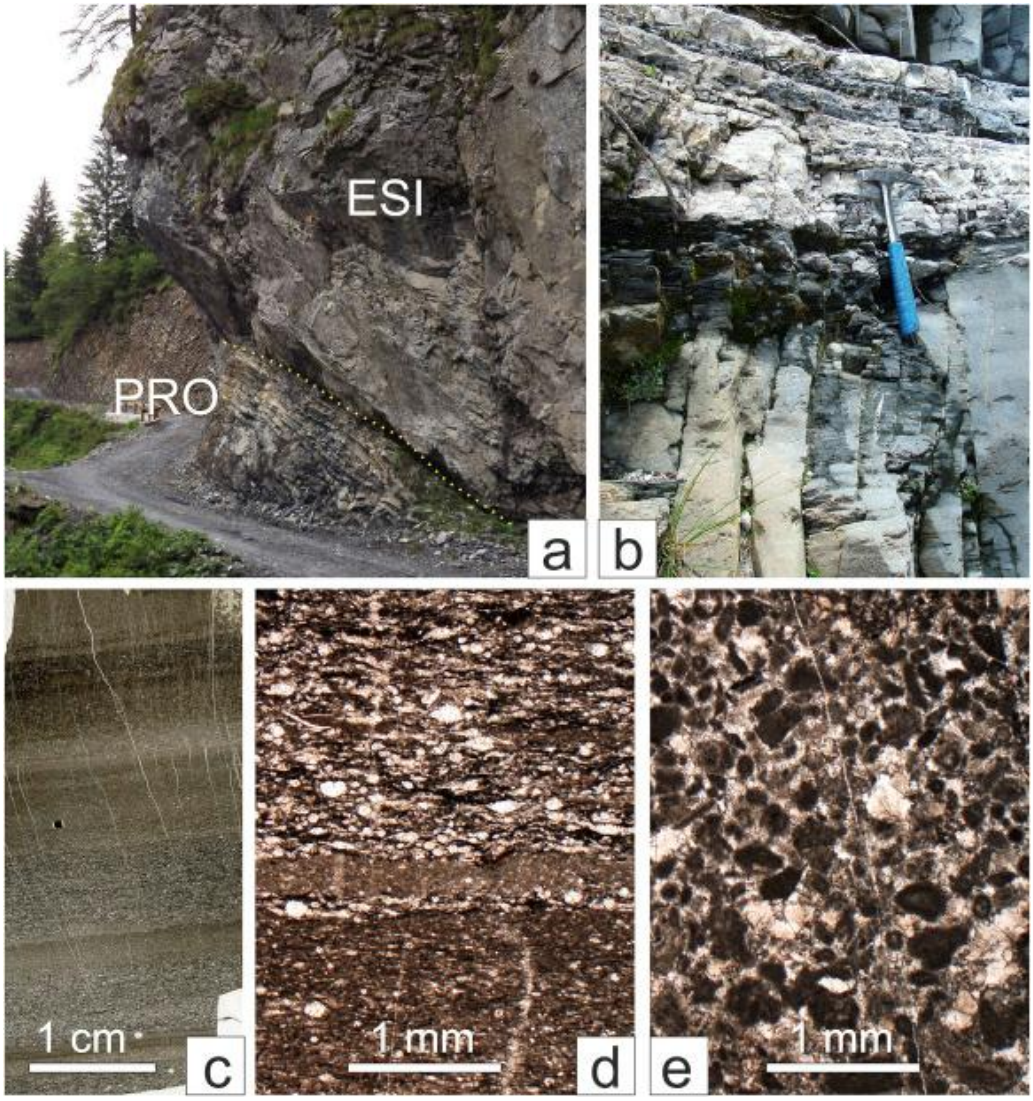

Fig. 9: Geometry facies and microfacies of the basinal sediments below the prograding Esino Limestone in different parts of the Lombardy Basin: a) sharp contact between the overlying massive slope breccias of the Esino Limestone (toe of the slope, ESI) and the underlying bedded limestone (locally affected by slumps, PRO); b) aspect of the basinal succession, with alternating marly (below) and calcareous horizons (above); c) thin section of laminated, fine grained calciturbidites, note that the fractures developed after compaction of the sediments; d) detail of “c”, wackestone/packstone with evidence of compaction of the fine-grained material mostly documented by flattened grains and compacted mud; e) intraclastic packstone, strongly packed (long and concavo-convex contacts, Taylor, 1950, can be observed among dark intraclasts) before the formation of the cement-filled fracture. The compaction in microfacies “d” is higher than in microfacies “e”. “a” and “b”, upper Val Brembana, “c” to “e”, Val Camonica.

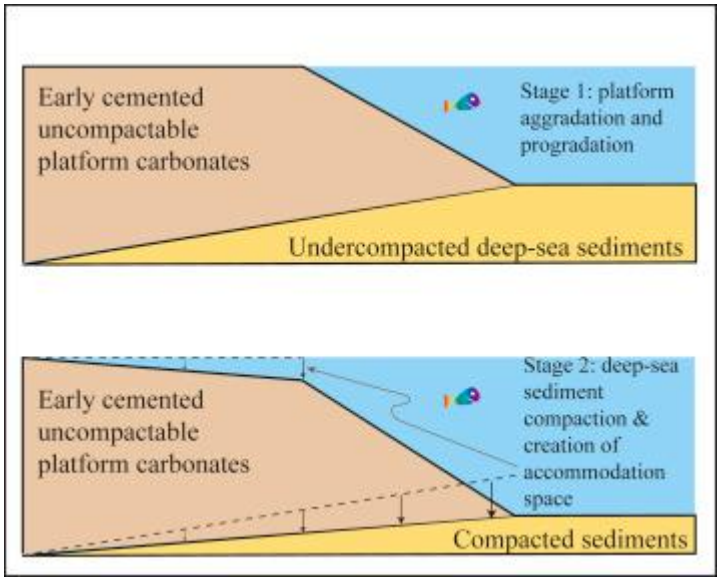

Fig. 10: Differential compaction of internal platform and platform slope sediments prograding onto compactable basinal sediments can lead to production of a wedge-shaped accommodation space on top of the carbonate platform after its demise.

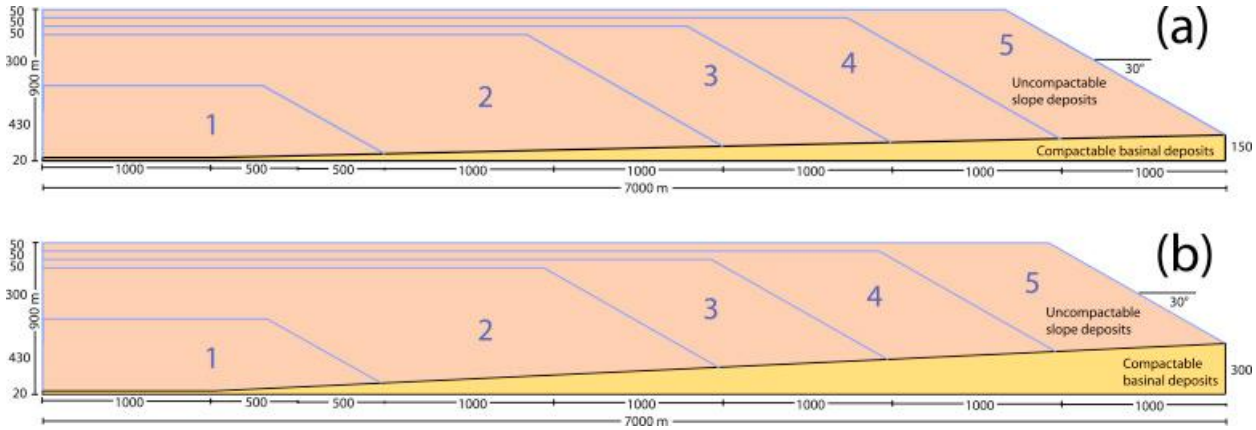

Fig. 11: Model geometry. Panels a and b show the two modelled scenarios, characterized by 150 m and 300 m maximum thickness of compactable basinal sediments respectively.

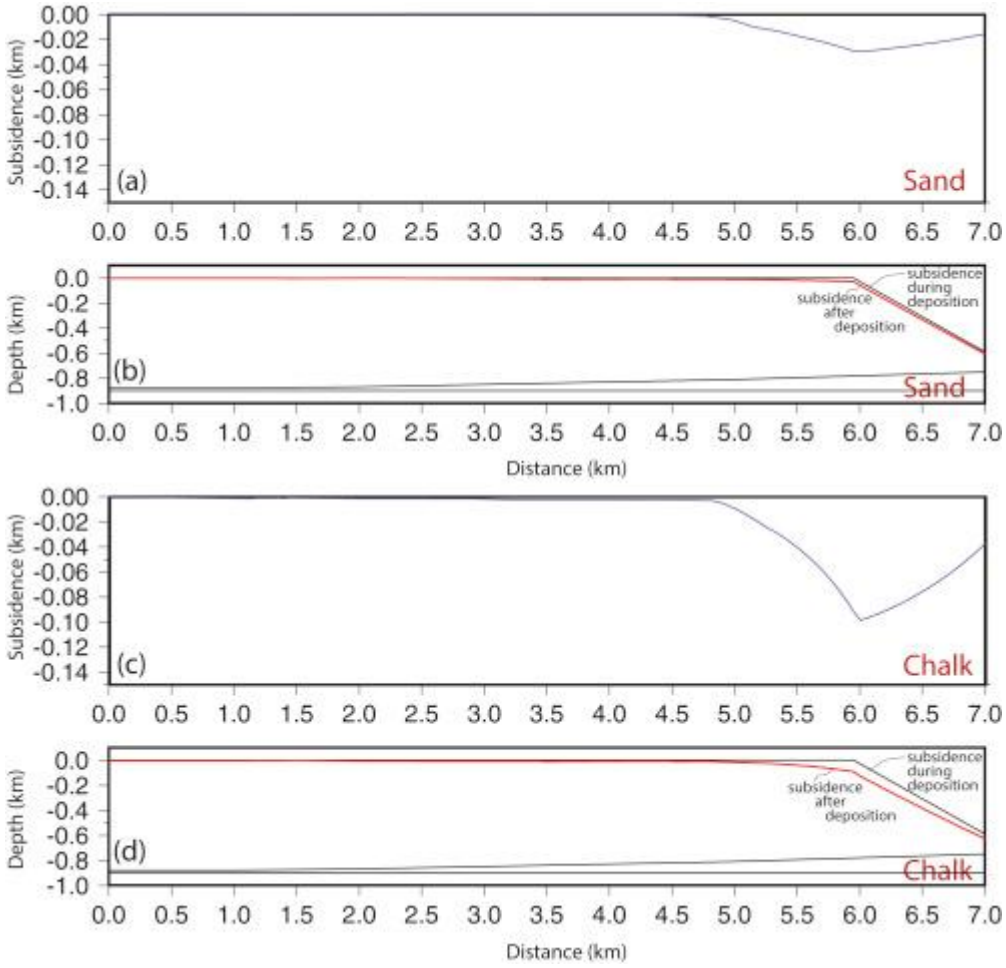

Fig. 12: Model results for the scenario characterized by 150 m thick compactable sediments. Panels a and c show the compaction induced by compaction of the basinal sediments, whereas panels b and c show the final geometry of the platform-basin system for sand and chalk lithologies, respectively.

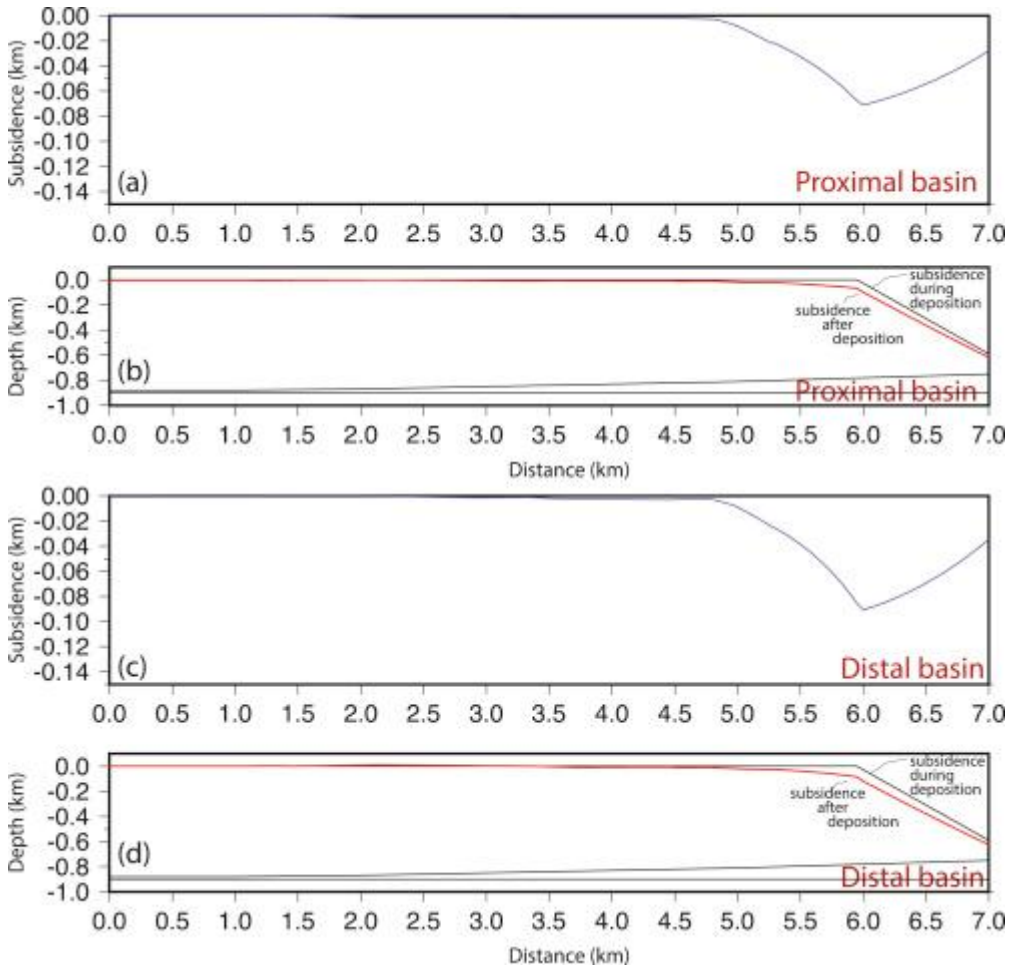

Fig. 13: Model results for the scenario characterized by 150 m thick compactable sediments. Panels a and c show the compaction induced by compaction of the basinal sediments, whereas panels b and c show the final geometry of the platform-basin system assuming compaction parameters for proximal and distal basins, respectively.

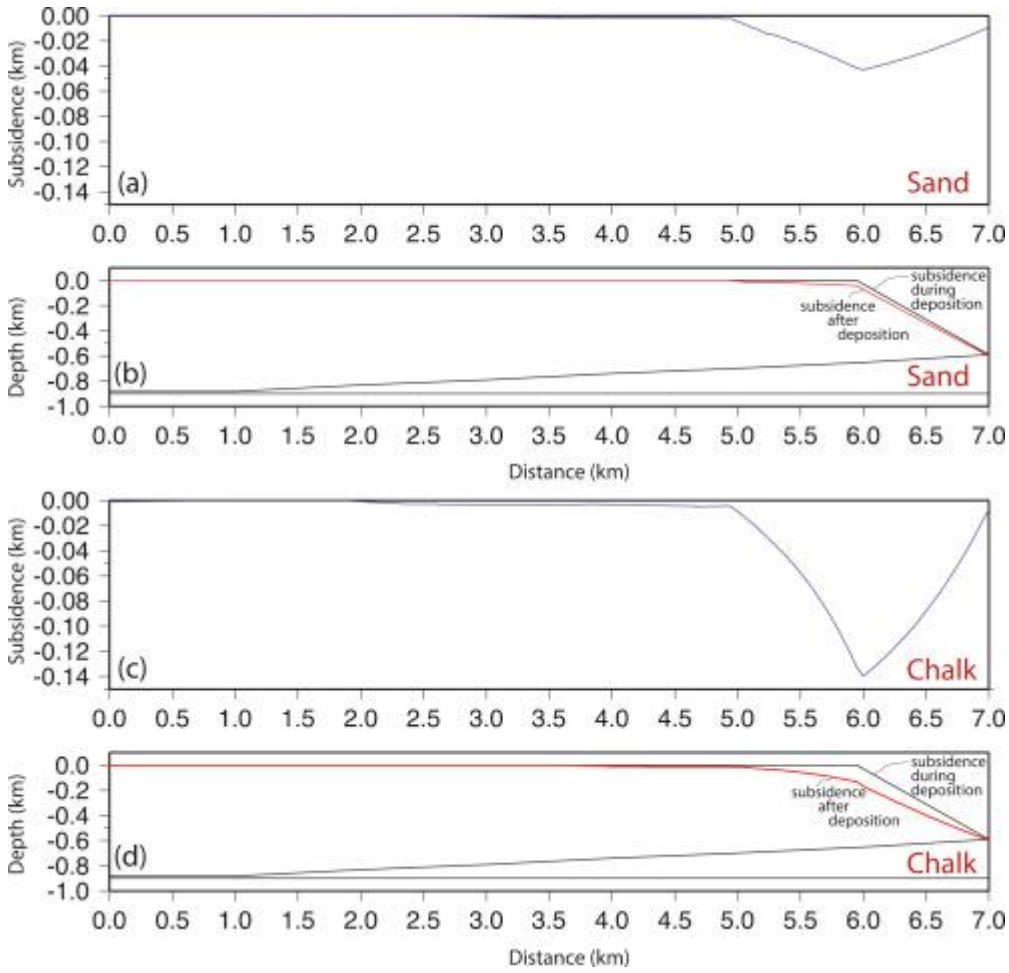

Fig. 14: Model results for the scenario characterized by 300 m thick compactable sediments. Panels a and c show the compaction induced by compaction of the basinal sediments, whereas panels b and c show the final geometry of the platform-basin system for sand and chalk lithologies, respectively.

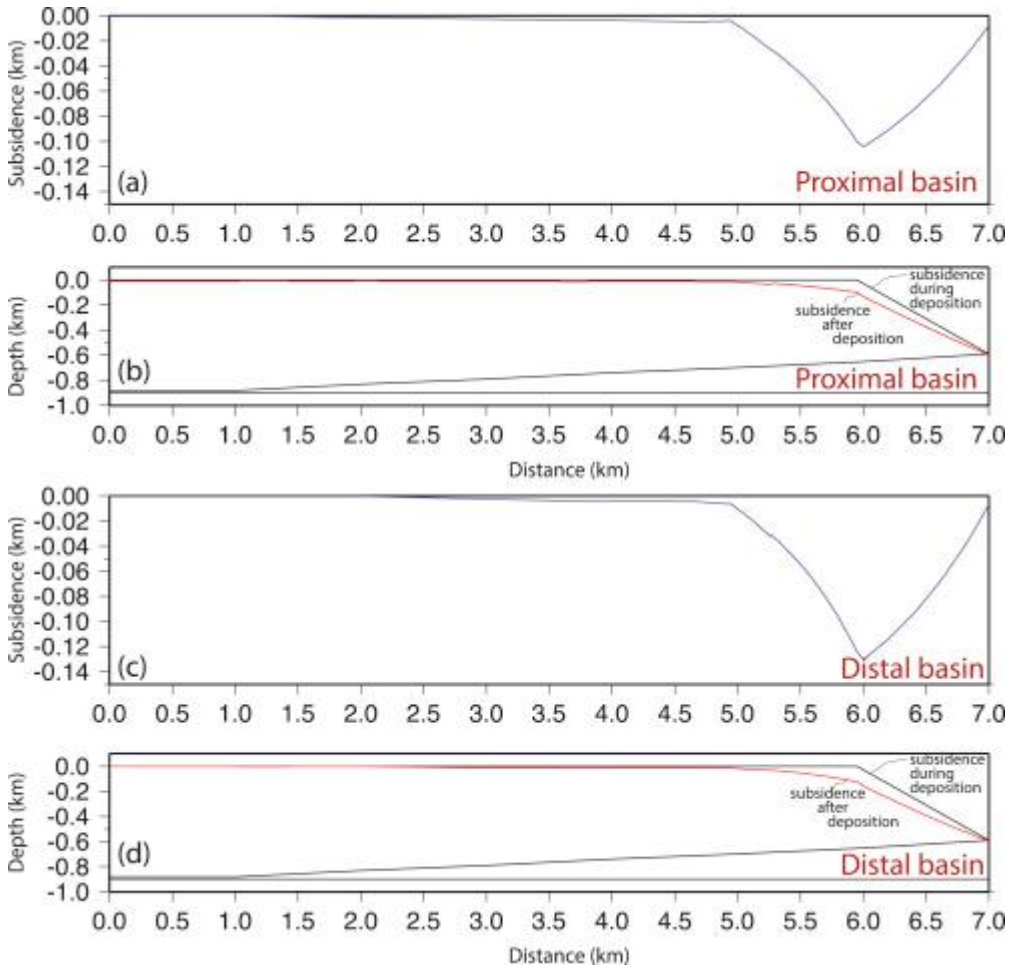

Fig. 15: Model results for the scenario characterized by 300 m thick compactable sediments. Panels a and c show the compaction induced by compaction of the basinal sediments, whereas panels b and c show the final geometry of the platform-basin system assuming compaction parameters for proximal and distal basins, respectively.

Formation name	c	ϕ	ρ	Lithology
Esino Limestone (uncompactable)	0.3	0.001	2710	100% limestone (early-cemented)
Fine basinal facies (Buchenstein Formation, Perledo-Varenna/Pratotondo Formations)	0.68	0.689	2711.5	85% micritic limestone; 15% pelite
Coarse basinal facies (Wengen Formation)	0.57	0.64	2696	60% micritic limestone; 15% pelite; 25% sandstone

Table 1 - Input parameters for the numerical model. c is the compaction coefficient, ϕ is the porosity at the surface and r is the grain density (km/m^3).